

1 Polarized Beam and Polarization Measurement

1.1 Deuteron polarized beam and asymmetries

The polarized ion source for spin-one deuteron beams changes the fraction, f_1 , f_0 , or f_{-1} , of the beam that is in each of the three magnetic substates away from the unpolarized values of $f_1 = f_0 = f_{-1} = 1/3$ [1]. This can produce either a vector polarization ($p_V = f_1 - f_{-1}$) and/or a tensor polarization ($p_T = 1 - 3f_0$) with respect to the orientation of the quantization axis established by the magnetic field in the ion source. With atomic beam sources [1] a pure vector polarization (with a very small tensor polarization or $f_0 = 1/3$) can reach values of $p_V = 0.6$; if a large tensor polarization is allowed, values may exceed $p_V = 0.9$ (with $f_1 \sim 1$).

Any possible EDM will be aligned along the direction of the particle spin. The coupling of the EDM to the electric field generated by $\mathbf{v} \times \mathbf{B}$ effects in the storage ring will reorient the particle spin direction, a phenomena that is most easily tracked by measuring the direction of the vector polarization of the deuteron beam. The polarization of a deuteron beam with an arbitrarily oriented quantization axis can be determined by measuring deuteron-induced reactions on a target, provided that the relevant analyzing powers (or sensitivities to the polarization) are sufficiently large.

Figure 1 shows the definition of the spin direction with respect to a coordinate system determined by the detected reaction product. The beam defines the positive \hat{z} axis. The location of the particle detector, along with the beam axis, defines the scattering plane and the direction of the positive \hat{x} axis. The scattering angle is β . In this coordinate system we can specify the orientation of the deuteron beam quantization axis by using the two angles of a spherical coordinate system, θ and ϕ , where ϕ is measured from the \hat{y} axis and increases toward the positive \hat{x} axis. The sensitivity of the reaction cross section at the detector to vector and tensor polarization is given by:

$$\begin{aligned}
 \sigma(\beta, \theta, \phi) &= \sigma_{\text{unp}}(\beta) \left[1 + \sqrt{3} p_V i T_{11}(\beta) \sin \theta \cos(\phi) \right. \\
 &+ \frac{1}{\sqrt{8}} p_T T_{20}(\beta) (3 \cos^2 \theta - 1) \\
 &- \sqrt{3} p_T T_{21}(\beta) \sin(\theta) \cos \theta \sin(\phi) \\
 &\left. - \frac{\sqrt{3}}{2} p_T T_{22}(\beta) \sin^2 \theta \cos 2\phi \right] .
 \end{aligned} \tag{1}$$

where the T_{kq} are the analyzing powers ($k = 1$ for vector, $k = 2$ for tensor). Both the unpolarized cross section and the analyzing powers are properties

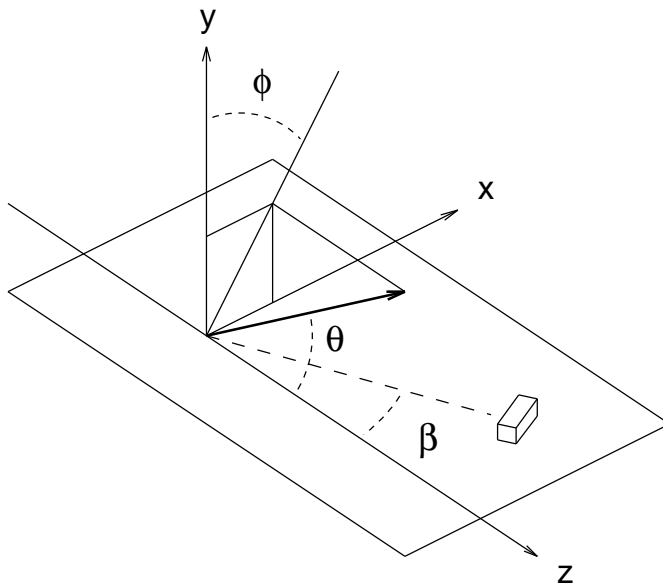


Figure 1: The coordinate system for polarization direction (heavy arrow) based on the observation of a reaction product in a detector (small box). The beam travels along the \hat{z} axis. The detector position at an angle β defines, along with the beam, the reaction plane and positive \hat{x} . The quantization axis for the polarization (heavy arrow) lies in a direction given by the polar angles θ and ϕ (as measured from the \hat{y} axis).

of the reaction.

The reaction is most sensitive to the vertical (along the \hat{y} axis) component of the vector polarization when $\cos \phi$ is near 1 or -1 . If both p_V and iT_{11} are positive, for example, then the rate at the detector (shown by the small box in Fig. 1) will increase relative to the unpolarized beam rate. Likewise, a detector on the opposite side of the beam (on the $-\hat{x}$ side) will see a reduced rate. (By rotating the plane of Fig. 1 about the \hat{z} axis, this detector can be placed at $+\hat{x}$ and then $\phi = 180^\circ$ and $\cos \phi = -1$.) The *asymmetry* in these two rates is a measure of the product $p_V iT_{11}$ and, for iT_{11} known, of the vertical component of p_V . If the left and right rates are L and R , then

$$p_{V,y} iT_{11}(\beta) = \epsilon_{LR} = \frac{L - R}{L + R}. \quad (2)$$

Over the length of a beam store, the size of $p_{V,y}$ will steadily increase due to the accumulated contributions from the interaction of the deuteron EDM

with the electric field. This is the signal that will reveal the presence of the EDM.

At the same time, there will be a large and oscillating \hat{x} component of the deuteron polarization due to the precession of the magnetic moment in the dipole fields of the ring. In a similar manner as described above, this will generate a difference in count rates for detectors mounted above and below the beam. So $p_{V,x} iT_{11}(\beta) = (D - U)/(D + U)$. This asymmetry will oscillate with the $g - 2$ frequency, and the accumulation of useful statistics will require that we synchronize the data collection to that frequency. In practice, we will use the synchrotron oscillation as observed from beam position in the dispersed region of the ring, and the observation of an asymmetry will confirm the correct locking of the phase and frequency to that of the $g - 2$ oscillation. Differences in the result from what is expected can be used to correct the driving frequency or phase.

A measurement of the longitudinal component of p_V is forbidden to the extent that the reaction process conserves parity. At similar energies per nucleon, small violations [2, 3] at the level of a few parts in 10^7 are seen for proton elastic scattering due to the interference between weak and strong interaction contributions.

1.2 Analyzing reaction

A measurement of p_V using scattering or reactions produced by passing the deuteron beam through a target leads to the search for target materials and processes with simultaneously large cross sections and vector analyzing powers. Most commonly, such effects are a result of the spin-orbit interaction between the deuteron and the nucleus. Cross sections are largest at forward angles, and the best process is usually elastic scattering. When compared across the periodic table, the largest effects are seen for the lighter masses unless few-body effects come to dominate. The choice of deuteron polarimeter builders [4, 5, 6] in this energy regime has been carbon, and that is what we suggest here. These authors have built and calibrated such instruments in the momentum range of $p = 1.0 - 1.5$ MeV/c (or kinetic energy $T = 250 - 526$ MeV) for use with secondary particles in a spectrometer system.

Figure 2 shows a sample of high-precision elastic scattering measurements at 270 MeV from the SMART spectrometer at RIKEN. As a function of increasing laboratory angle β , the cross section falls steadily and quickly while the vector analyzing power iT_{11} shows two interference maxima and is always positive. While $iT_{11}(\beta)$ must vanish at $\beta = 0$, for the angles

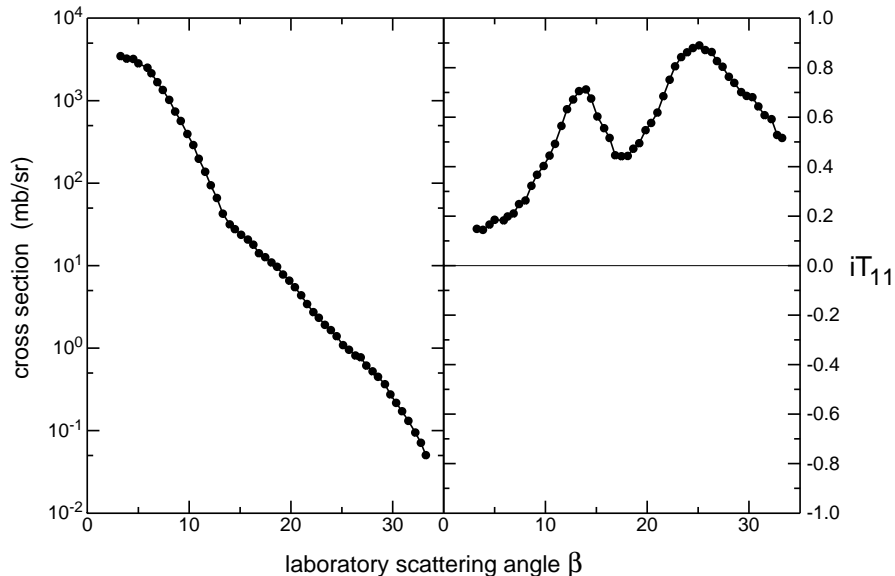


Figure 2: Measurements of deuteron elastic scattering cross section and vector analyzing power iT_{11} from carbon at 270 MeV made with the SMART spectrometer at RIKEN. Errors are not shown.

shown here the vector analyzing power is always a significant fraction of its maximum possible value of 1.

The detector acceptance is chosen to span a range of angles that will provide a good statistical basis for the polarization measurement. In choosing the best angle range, we must balance the large cross section found at small angles against the larger values of $iT_{11}(\beta)$ found at the larger angles. This becomes a trade-off between higher counting rate and sensitivity to p_V . The statistical part of the trade-off can be quantified by introducing a *figure of merit* which is defined by [4, 5]

$$FOM(\beta) = \sqrt{\sigma_{\text{unp}}(\beta)} iT_{11}(\beta) . \quad (3)$$

This quantity is proportional to $1/\delta$ where δ is the error in the measurement of the polarization components of p_V for a fixed time and beam on target. In addition, the sensitivity to systematic errors is reduced if the analyzing power is larger. This trade-off is illustrated in Fig. 3 which plots $iT_{11}(\beta)$ against $FOM(\beta)$. Statistical efficiency would favor using angles less than about 11° while a larger analyzing power would suggest monitoring only angles greater than about 11° .

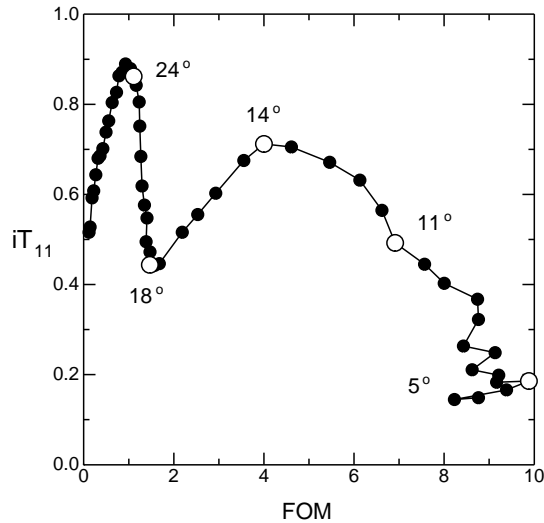


Figure 3: Plot of the analyzing power iT_{11} against the figure of merit. The curve connects points at neighboring angles. Angles whose value is close to an integer are shown as open points and the angle written close to the point. Errors are not shown.

We are considering designs for the storage ring that have deuteron momenta between 1.0 and 1.5 GeV/c, so it is important to know how maximizing either figure of merit or analyzing power would depend on the choice of momentum. As shown in Fig. 3, near 1 GeV/c these two choices lead to different angle coverage. But as the momentum rises, the peak in the analyzing power move toward smaller scattering angles and these choices merge. In Fig. 4, the solid dots show the momentum dependence of the figure of merit, the analyzing power, and the polarimeter efficiency (into all azimuthal angles, even though only half contribute to either the horizontal or vertical asymmetry) averaged over the range of acceptable angles (usually spanning 5° to 10°) when the angle range follows the figure of merit peak. As the momentum increases, the thickness of the carbon target can also increase since the deuterons have a longer range. Over this plot the thickness varies from 3.8 to 27.4 cm. (The thicknesses at 1.0 and 1.5 GeV/c are 4.4 and 15 cm.) The cross sections actually go down with increasing momentum, leading to an efficiency that is nearly flat. The efficiency is the number of scattered deuterons that are captured within the detector acceptance (and thus are useful for a measurement) divided by the number of deuterons striking the target. Thus the shape of the figure of merit curve is

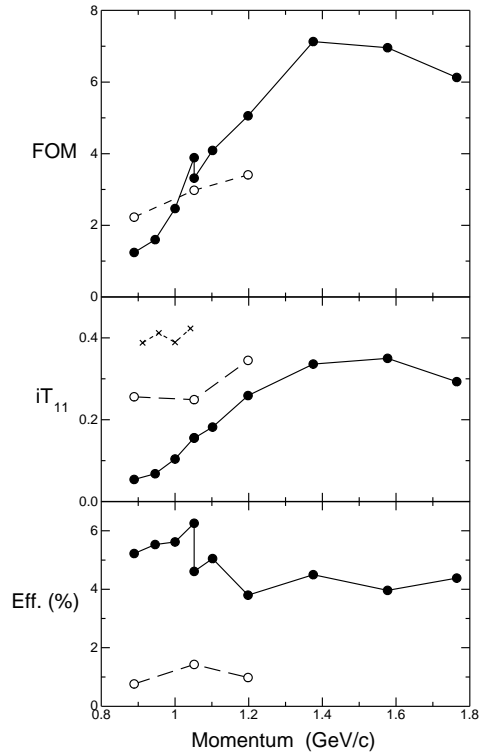


Figure 4: Variation of the figure of merit, average analyzing power, and polarimeter efficiency as a function of the momentum of the deuteron storage ring. Solid points track an angle range that covers the largest figure of merit values at small scattering angles. The open circles show an alternative that emphasizes larger analyzing powers. The X-points show the analyzing power with better discrimination against breakup protons. Errors are not shown.

determined solely by the analyzing power. At the lowest momenta, we can shift the range of angles in the acceptance to the analyzing power peak and regain enough statistical information that we eventually outstrip the cross section losses at larger angle and produce a higher figure of merit (open points). When this occurs, there are two $FOM(\beta)$ peaks as a function of the scattering angle β . The choice will depend in part on constraints at the smaller angles in the construction of the polarimeter and estimates of the importance of systematic errors in the final design.

1.3 Polarimeter components

The design of the polarimeter depends on the final determination of its location. One option considered for an earlier version of this experiment was to place the polarimeter components along the storage ring itself and to use small angle Coulomb scattering to extract particles from the beam. Once extracted, particles would then strike an annular target that surrounds the beam and from which they would scatter into the detector system. Variations on this scheme include creating a spatial bump in the beam to bring particles to the target, or moving the target into the beam continuously during the store. A second class of options is generated by constructing a standard slow extraction system that transports deuterons to the polarimeter, which would then be external to the ring.

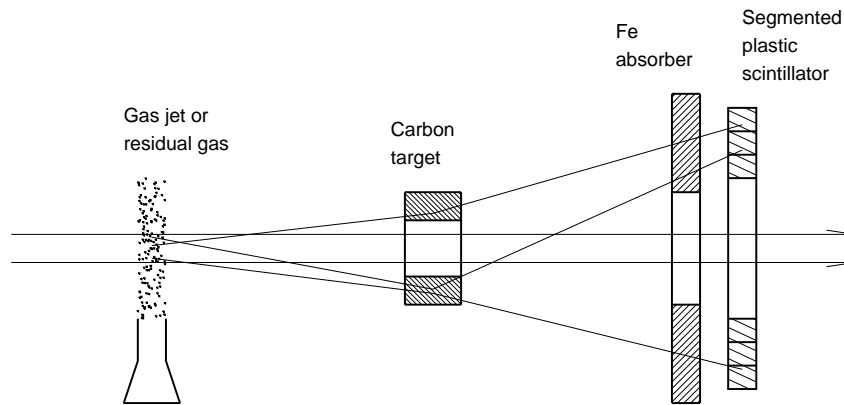


Figure 5: Schematic layout (not to scale) of the major components of the polarimeter if it were situated on the ring. The beam travels from left to right. Coulomb scattering from a gas jet (or residual gas) sends some deuterons to an annular carbon target that also defines the ring aperture. Larger angle elastically scattered deuterons proceed through an iron absorber that reduces non-elastic backgrounds and then into a segmented scintillator.

A schematic layout of the polarimeter is presented in Fig. 5 which shows the major components as they might appear if the polarimeter were located on the ring. The aim of this scheme is to transport deuterons to the carbon target continuously during the store, and to have that carbon target be thick so that the polarimeter maintains high efficiency. One scheme for achieving this would be to introduce a thin target gas (Ar, for example) from which

a few of the deuterons in the beam would scatter in the Coulomb field of the nucleus or the atomic electrons much as they do in the standard multiple scattering energy loss process that takes place when they enter matter. Downstream of this point, perhaps one to a few meters, the polarimeter carbon target in the shape of an annulus about the beam would be installed. The Coulomb scattered deuterons would hit this target and be removed from the beam. This amounts to slow extraction. Inside the target the deuterons would scatter again in the strong field of the carbon nuclei and travel to some part of a segmented plastic scintillator target downstream. The carbon target itself could be cut into sections and pulled away from the beam during the injection cycle and replaced when it was time to begin observations.

This scheme has the advantage of sampling uniformly across the entire beam and providing a way to control rates and beam lifetime through changes in the gas target density. Depending on the details of the design, some scattering will also occur from residual gas in the vacuum of the ring. If this rate is high enough in the final geometry, a separate gas target may not be needed. In both situations, the annular target is the defining aperture for the ring. Thus any stray particles will be lost at this point. This is crucial for maintaining high efficiency in the sampling of the deuteron beam for a polarization measurement. Some deuterons will strike the carbon target along the inner surface that faces the beam, and thus not take full advantage of the carbon target thickness for their larger angle scattering. They will nevertheless be removed from the beam.

It is possible that larger angle scattering to the left or right from the gas target could induce a vertical polarization of these deuterons. Any effect on the measurement is suppressed by maintaining the symmetry of the geometry, a problem that will be discussed in a later section on systematic errors.

Both deuteron polarimeter efforts [4, 5, 6] found that it was efficacious to remove most non-elastic particles from the scattered flux before they reached the detector. This was achieved in both cases with the addition of an iron absorber between the carbon target and the detectors. Thicknesses between 1.0 and 1.5 GeV/c ranged from 2 to 7 cm [4]. The main effect is to remove essentially all of the breakup protons, which have only a tiny spin dependence, from the data sample. Bonin and Satou chose different optimizations for this absorber thickness. Bonin allowed some breakup proton flux. Satou optimized for selection of just the elastic group. Thus the Satou analyzing powers are larger, as shown by the points marked with an \times in Fig. 4. But this gain came at the expense of at least a factor of two in rate,

so the figures of merit of the French and Japanese systems are comparable. The optimization of this thickness is an important aspect of the design, just as is the choice of the angular acceptance range.

The detector must be chosen to deal with large rates and precise timing. If there are 10^{11} deuterons in a fill and we extract half during a 500 s store, the rate into the carbon target is 10^8 /s. The efficiencies shown in Fig. 4 would then yield 5×10^6 /s into the whole detector, not considering background. Thus it is important to reduce rates as much as possible before the detector. While a layered detector can be used to make particle identification, the elastic deuterons will be the highest energy events recorded here. Complete discrimination against all backgrounds is not a requirement, as the operating parameters of the polarimeter and the spin dependence that results will be calibrated separately. We only require that the response of the polarimeter is stable and reproducible. Some contamination of the signal is acceptable provided the performance is not compromised.

Functionally, the detector is divided into four quadrants that produce two asymmetries from the comparison of left with right, and down with up, rates. Practically, division into more segments (approximately 50) is desirable, with slices in both θ and ϕ . Segmentation in ϕ will allow the division into samples for each quadrant to be made in the analysis, thus reducing effects of cross talk from small rotations of the detector segments about the beam. Segmentation in θ angle allows comparison of forward angle results where statistics and sensitivity to the geometric systematics are both large with larger angles where systematic effects are suppressed by the larger analyzing power. Finally, segmentation is also helpful with the management of readout rates.

We plan to have a large number (up to 40) RF buckets around the ring, thus beam bunches may pass through the polarimeter and be separated by times as small as 4 ns. In order to determine the phase relationship between the forced synchrotron oscillations and the $g - 2$ precession, we will need to determine unambiguously which bunch generated which polarimeter event. Thus timing at or below the nanosecond level is also a requirement that is met by the choice of plastic scintillator as the active detector element.

If a standard extraction scheme is used to remove deuterons from the storage ring, then there would be no need for the gas target. The extracted beam would pass directly into a carbon target with no hole. Scattered deuterons would be detected in the same detector arrangement.

References

- [1] W. Haeberli, *Ann. Rev. Nucl. Sci.* **17**, 373 (1967).
- [2] S. Kistryn *et al.*, *Phys. Rev. Lett.* **58**, 1616 (1987).
- [3] J. Lang *et al.*, *Phys. Rev. C* **34**, 1545 (1986).
- [4] B. Bonin *et al.*, *Nucl. Instrum. Methods* **A288**, 389 (1990).
- [5] V.P. Ladygin *et al.* *Nucl. Instrum. and Methods* **A404**, 129 (1998).
- [6] Y. Satou, private communication.